Supporting Information

Castañeda et al. 10.1073/pnas.0905771106

SI Text

Age Model of GeoB9528-3. The age model of GeoB9528-3 was constructed by visual correlation of the benthic foraminifer *C. wuellerstorfi* $\delta^{18}O$ record with the $\delta^{18}O$ records of marine sediment core MD95-2042 (1) and the global benthic $\delta^{18}O$ stack of Lisiecki and Raymo (2). The software package AnalySeries 1.1 (3) was used to perform peak-to-peak correlation, which was done on the smoothed (five-point running mean) $\delta^{18}O$ records. The $\delta^{18}O$ record of GeoB9528-3 was first correlated to the record of MD95-2042 (1) in the time interval spanning from 0 to ≈140 ka, and the older part of the record was correlated to the global benthic stack (2) in the time interval from ≈140 to 192 ka (Fig. S1). The benthic $\delta^{18}O$ record of GeoB9528-3 exhibits a close correlation with both the records of MD95-2042 (1) (R^2 = 0.91) and the global benthic stack (2) (R^2 = 0.93) (Fig. S1), attesting to the strength to the chronology.

Long-Chain *n*-Alkane $\delta^{13}C$ Values for C_3 and C_4 Plants. To estimate the past contribution of C_3 and C_4 vegetation to the different *n*-alkanes, we compiled a list of *n*-alkane $\delta^{13}C$ values reported for C_3 and C_4 plants in the literature (Table S1 and Table S2) (4-7). The mean values of C_{29} *n*-alkanes are −34.7‰ (n = 50) and −21.4‰ (n = 49) for C_3 and C_4 plants, respectively. The mean values of C_{31} *n*-alkanes are −35.2‰ (n = 52) and −21.7‰ (n = 50) for C_3 and C_4 plants, respectively. We use these mean end-members for C_3 and C_4 plants to create a binary mixing models to estimate the contribution of C_4 plants to the C_{29} and C_{31} *n*-alkanes, respectively. There is likely substantial error associated with the %C_4 estimates. The largest *n*-alkane $\delta^{13}C$ standard deviation of 2.6, which is reported for the C_{29} and C_{31} *n*-alkanes of C_3 plants (Table S1 and Table S2), translates to a maximum error estimate of ± 20% C_4 plants. However, for the purpose of our study, the overall trends in the *n*-alkane $\delta^{13}C$ records are more important than the %C_4 estimates because relatively enriched (depleted) *n*-alkane $\delta^{13}C$ values indicate increased (decreased) inputs from C_4 plants. Therefore, shifts to relatively enriched or depleted *n*-alkane $\delta^{13}C$ values provide important information on past vegetation shifts in central North Africa.

A Dust Source for Long-Chain Odd-Numbered *n*-Alkanes. Long-chain, odd-numbered *n*-alkanes (C_{25}–C_{35}) are a main component of plant epicuticular leaf waxes (8), and these compounds are generally well preserved in sediments. The carbon isotopic composition of *n*-alkanes can be used to distinguish between plants using the different photosynthetic pathways because C_4 plants, such as warm-season grasses, possess a CO_2 concentrating mechanism, which causes them to be isotopically enriched in ^{13}C compared with C_3 plants, which include most trees, cool-season grasses, and sedges. A third photosynthetic pathway, the CAM pathway, has isotopic values intermediate between those of C_3 and C_4 plants but CAM plants are not a significant component of northwest African vegetation (9).

Although long-chain *n*-alkanes are produced by higher plants, these compounds are also found in petroleum. However, the *n*-alkane carbon preference index (CPI) (10), which is used to examine odd over even carbon number predominance, can be used to distinguish terrestrial plant from petroleum sources. Terrestrial plants are characterized by CPIs of >3, whereas mature hydrocarbons have CPIs of ≈1 (10). Core GeoB9528-3 is characterized by high CPI values, which range from 3.5 to 8.3 with a mean value of 6.2, indicating a source from terrestrial higher plants throughout the entire record (8).

Plant leaf waxes (*n*-alkanes) can be transported to marine sediments by wind or water (runoff or riverine inputs); however, fluvial transport is not likely at site GeoB9528-3. The coring site is located offshore on the continental slope with no major rivers in close vicinity. Furthermore, we analyzed core GeoB9528-3 for branched glycerol dialkyl glycerol tetraethers (GDGTs), which are lipids produced by soil bacteria that are transported solely by runoff/riverine input (11). However, branched GDGTs were not detected in GeoB9528-3. Thus, the main supply of *n*-alkanes to GeoB9528-3 is via wind erosion.

Origin of Dust and Associated Leaf Wax *n*-Alkanes Transported to Site GeoB9528-3. The main source of *n*-alkanes to site GeoB9528-3 is from the central Africa near the boundary of the Sahara with the Sahel (Fig. 1). Isotopic mapping of *n*-alkanes in dust (12) and surface sediments (13) collected off the coast of Northwest Africa supports this hypothesis. The isotopic pattern in surface sediments of Northwest Africa depends in the latitudinal distribution of vegetation and the transport pathways of the wind systems. Enriched *n*-alkane $\delta^{13}C$ values, indicating high C_4 contributions, are noted in both dust and surface sediments offshore Northwest Africa between ≈0 and 10°N (12, 13), although at this latitude the adjacent continent is covered by tree savanna or rainforest, which is C_3 dominated. This pattern is attributed to long-distance transport of Saharan dust to offshore Northwest Africa (12, 13). Modeling of backwards trajectories indicates that the dust reaching 10°N (near the location of GeoB9528-3) originates from central Africa near the boundary of the Sahara with the Sahel (12). Thus, this region of central North Africa is likely the main source of *n*-alkanes to site GeoB9528-3.

Relationship Between $\delta^{13}C_{\text{benthic}}$ and *n*-Alkane $\delta^{13}C$. Throughout the past 200 ka, a significant negative linear relationship is observed between $\delta^{13}C_{\text{benthic}}$ and the *n*-alkane $\delta^{13}C$ records of GeoB9528-3 (Fig. S2; $R^2 = -0.79$ for the C_{29} *n*-alkane and −0.82 for the C_{31} *n*-alkane;), indicating a strong association between AMOC strength and vegetation type in the Sahara/Sahel region.

Alkenone SST Estimates. Molecular identification of the $C_{37:2}$ and $C_{37:3}$ alkenones was performed on a Thermo Finnigan Trace Gas Chromatograph Ultra coupled to Thermo Finnigan DSQ mass spectrometer. A 25-m CP Sil-5 fused silica capillary column was used (25 m × 0.32 mm; film thickness = 0.12 μm) with helium as the carrier gas. The column was directly inserted into the electron impact ion source of the DSQ quadrupole mass spectrometer. Mass scans were made in the range of m/z = 50–800 with three scans per s and an ionization energy of 70 eV. The temperature program initiated at 70 °C, increased first at a rate of 20 °C per min to 130 °C, and next at a rate of 4 °C min to the final temperature of 320 °C, which was held for 10 min.

For quantification, samples were analyzed on an HP 6890 GC using a 50-m CP Sil-5 column (0.32-mm diameter, film thickness of 0.12 μm) and helium as the carrier gas. The oven program initiated at 70 °C and increased by a rate of increased by 20 °C per min to 200 °C and next by a rate of 3 °C per min until 320 °C. The final temperature of 320 °C was held for 25 min. Compound concentrations were determined by relating chromatogram peak areas to the concentration of the internal standard.

The $U^{k'}_{37}$ Index, defined as $C_{37:2}/(C_{37:2} + C_{37:3})$, was used to estimate SSTs (14). $U^{k'}_{37}$ values were converted to SSTs by using the core top calibration of Müller et al. (15). Of the 193 samples analyzed, 74 were run in duplicate and 18 were run in triplicate. The reproducibility of these analyses is always better than ± 0.6 °C.

1. Shackleton NJ, Fairbanks RG, Chiu TC, Parrenin F (2004) Absolute calibration of the Greenland time scale: Implications for Antarctic time scales and for $\Delta^{14}C$. *Q Sci Rev* 23:1513–1522.
2. Lisiecki LE, Raymo ME (2005) A Pliocene-Pleistocene stack of 57 globally distributed benthic $\delta^{18}O$ records. *Paleoceanography* 20:PA1003, 10.1029/2004PA001071.
3. Paillard D, Labeyrie L, Yiou P (1996) Macintosh program performs time-series analysis. *Eos* 77:379.
4. Collister JW, Rieley G, Stern B, Eglinton G, Fry B (1994) Compound-specific $\delta^{13}C$ analyses of leaf lipids from plants with differing carbon dioxide metabolisms. *Org Geochem* 21:619–627.
5. Bi XH, Sheng GY, Liu XH, Li C, Fu JM (2005) Molecular and carbon and hydrogen isotopic composition of *n*-alkanes in plant leaf waxes. *Org Geochem* 36:1405–1417.
6. Chikaraishi Y, Naraoka H (2003) Compound-specific δD-$\delta^{13}C$ analyses of *n*-alkanes extracted from terrestrial and aquatic plants. *Phytochemistry* 63:361–371.
7. Rommerskirchen F, Plader A, Eglinton G, Chikaraishi Y, Rullkotter J (2006) Chemotaxonomic significance of distribution and stable carbon isotopic composition of long-chain alkanes and alkan-1-ols in C_4 grass waxes. *Org Geochem* 37:1303–1332.
8. Eglinton G, Hamilton RJ (1967) Leaf epicuticular waxes. *Science* 156:1322–1335.
9. Winter K, Smith JA (1996) *Crassulacean Acid Metabolism: Biochemistry, Ecophysiology, and Evolution* (Springer, Berlin).
10. Bray EE, Evans ED (1961) Distribution of normal paraffins as a clue to recognition of source beds. *Geochim Cosmochim Acta* 22:2–15.
11. Weijers JWH, Schouten S, van den Donker JC, Hopmans EC, Sinninghe Damsté JS (2007) Environmental controls on bacterial tetraether membrane lipid distribution in soils. *Geochim Cosmochim Acta* 71:703–713.
12. Schefuß E, Ratmeyer V, Stuut J-BW, Jansen JHF, Sinninghe Damsté JS (2003) Carbon isotope analyses of *n*-alkanes in dust from the lower atmosphere over the central eastern Atlantic. *Geochim Cosmochim Acta* 67:1757–1767.
13. Huang YS, Dupont L, Sarnthein M, Hayes JM, Eglinton G (2000) Mapping of C_4 plant input from North West Africa into North East Atlantic sediments. *Geochim Cosmochim Acta* 64:3505–3513.
14. Prahl FG, Muehlhausen LA, Zahnle DB (1988) Further evaluation of long-chain alkenones as indicators of paleoceanographic conditions. *Geochim Cosmochim Acta* 52:2303–2310.
15. Müller P, Kirst G, Ruhland G, von Storch I, Rosell-Melé A (1998) Calibration of the alkenone palaeotemperature index $U^{k'}_{37}$ based on core-tops from the eastern South Atlantic and the global ocean (60ºN-60ºS). *Geochim Cosmochim Acta* 62:1757–1772.

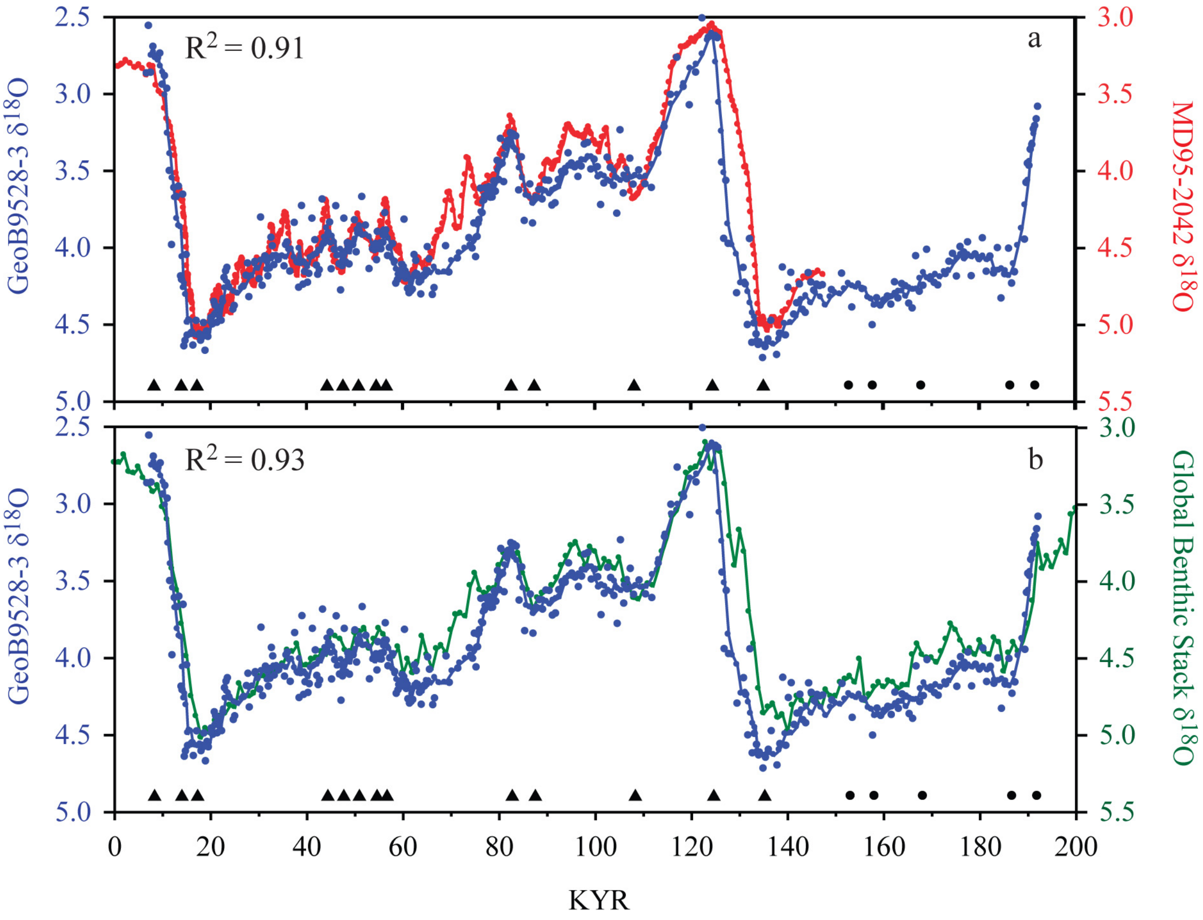

Fig. S1. Age model of GeoB9528-3. The benthic (*C. wuellerstorfi*) δ^{18}O record of GeoB9528-3 is shown in blue. The blue circles indicate all δ^{18}O measurements while the blue line represents the smoothed data (five-point running mean). The triangles at the bottom of the graph indicate the tie points to the benthic record of MD95-2042 (1), and the circles indicate the tie points to the global benthic stack (2). (*a*) Cross-correlation between the δ^{18}O records of GeoB9528-3 and MD95-2042 (plotted in red) (1). (*b*) Cross-correlation between the δ^{18}O record of GeoB9528-3 and the global benthic stack (plotted in green) (2).

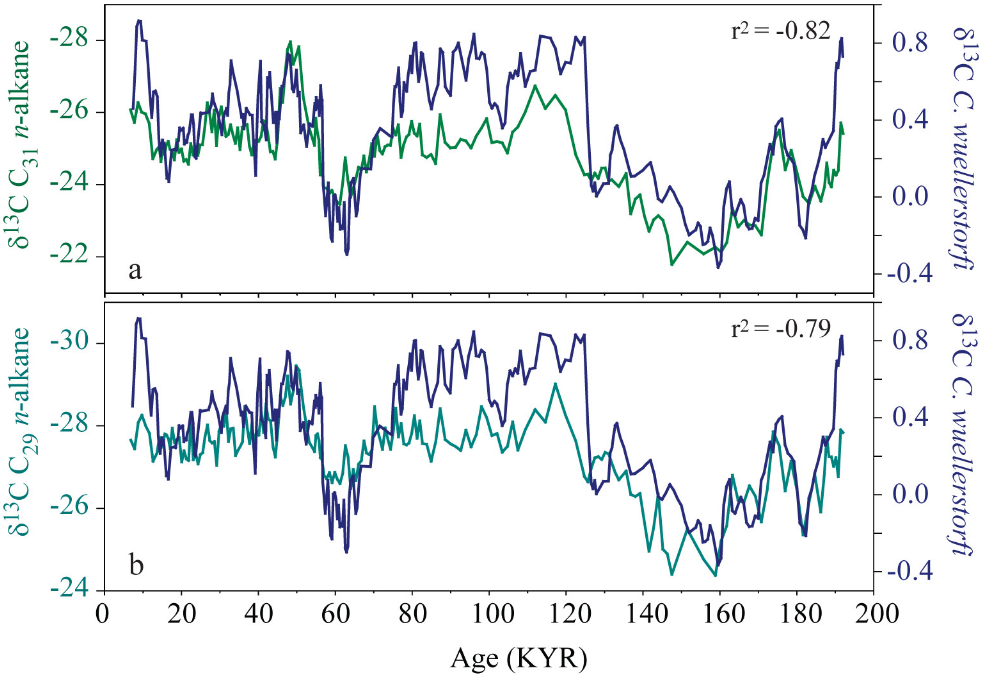

Fig. S2. Cross-correlation between the *n*-alkane $\delta^{13}C$ records and the $\delta^{13}C$ record of *C. wuellerstorfi* of GeoB9528–3. The benthic (*C. wuellerstorfi*) $\delta^{13}C$ record of GeoB9528-3 is shown in dark blue. In *a*, the $\delta^{13}C_{31}$ record is plotted in green, and in *b*, the $\delta^{13}C_{31}$ record is plotted in light blue.

Table S1. Carbon isotopic values ($\delta^{13}C$) of the C_{29} and C_{31} *n*-alkanes of C_3 plants

Plant	Type	$\delta^{13}C_{29}$, $n = 50$	$\delta^{13}C_{31}$, $n = 52$	Ref.
Psidium cattleionum	C3	−38.6	−38.8	4
Jacobinia cornea	C3	−36.1	−36.2	4
Cyperus diffusus	C3	−36.2	−36.5	4
Dendrocalamus stricus	C3	−35.3	−36.4	4
Cyprus alternifolius	C3	−34.2	−35.3	4
Fagus sylvatica	C3			4
Acer campestre	C3	−35.0	−35.0	4
Magnolia delabayi	C3	−34.0	−34.3	4
Quercus turneri	C3	−32.9	−35.7	4
Quercus rober	C3	−36.4	−36.9	4
Euphorbia pulcherrima Willd.	C3	−38.0	−37.4	5
Codiaeum variegatum (L.) Bl. Var. *pictum* M.-A. forma *crispum* Pax	C3		−35.1	5
Ficus altissima Bl.	C3	−33.9	−36.1	5
Ficus microcarpa Linn. f.	C3	−31.0	−33.4	5
Osmanthus fragrans Lour.	C3	−35.7	−37.0	5
Kigelia africana (am.) Benth.	C3	−33.1	−33.3	5
Syzygium cumini (L.) Skeels	C3	−37.2	−35.5	5
Swietenia mahagoni (L.) Jacq.	C3	−34.1	−35.9	5
Pistia stratiotes	C3	−36.6	−37.1	5
Caryota mitis Lour.	C3		−35.5	5
Cinnamomum burmanni (Nees) Bl.	C3	−33.3	−37.2	5
Araucaria cunninghamii Sweet	C3	−30.1	−30.5	5
Alternanthera dentata 'Rubiginosa'	C3	−36.6	−37.2	5
Alternanthera versicolor Regel	C3	−36.7	−37.5	5
Alternanthera bettzickiana (Regel) Nichols.	C3	−36.5	−37.2	5
Holmskioldia sanguinea Retz.	C3	−35.3	−33.8	5
Quercus acutissima	C3	−34.7	−34.8	6
Camellia sasanqua	C3	−31.3	−33.1	6
Chamaecyparis obtusa	C3	−30.6	−30.0	6
Pinus thunbergii	C3	−33.5	−34.1	6
Colocasia esculenta	C3	−33.2	−34.0	6
Lycoris radiata	C3	−28.0	−28.4	6
Albizia julibrissin	C3	−35.9	−37.8	6
Benthamidia japonica	C3	−36.5	−36.5	6
Cryptomeria japonica	C3	−32.3	−30.4	6
Acer carpinifolium	C3	−35.5	−35.4	6
Acer argutum	C3	−35.9	−36.4	6
Phrogmites communis	C3	−34.6	−38.1	6
Benthamidia japonica	C3	−38.8	−37.3	6
Prunus jamasakura	C3	−34.2	−33.5	6
Cryptomeria japonica	C3	−32.9	−32.5	6
Acer carpinifolium	C3	−37.3	−37.1	6
Acer argutum	C3	−35.6	−36.0	6
Taraxacum officinale	C3	−37.0	−36.4	6
Plantago asiatica	C3	−39.6	−39.8	6
Artemisia princeps	C3	−36.5	−35.2	6
Acer palmatum	C3	−40.5	−41.8	6
Quercus mongolica	C3	−33.4	−32.2	6
Quercus dentata	C3	−33.5	−34.4	6
Manihot utilissima	C3	−30.8	−32.0	6
Bromus sp.	C3	−35.7	−36	7
Festuca orthophylla	C3	−30.3	−31.3	7
Festuca orthophylla	C3	−31.2	−32.2	7
Average		−34.7	−35.2	
SD		2.6	2.6	

Table S2. Carbon isotopic values ($\delta^{13}C$) of the C_{29} and C_{31} *n*-alkanes of C_4 plants

Plant	Type	$\delta^{13}C_{29}$, $n = 49$	$\delta^{13}C_{31}$, $n = 50$	Ref.
Saccharum officinarum	C4	−24.5	−23.4	4
Miscanthuys sacchariflorum	C4	−18.4	−18.4	4
Zea mays	C4		−20.5	4
Zea mays (L)	C4	−21.3	−22.1	5
Amaranthus tricolor (L)	C4	−25.8	−23.4	5
Amaranthus paniculatus (L)	C4	−25.4	−22.9	5
Imperata cylindrica var. *major* (Ness) C.E. Hubb.	C4	−21.0	−19.2	5
Bothriochloa ischaemum Keng	C4	−21.0	−22.1	5
Zoysia japonica Stued	C4	−24.1	−23.4	5
Saccharum sinense Roxb.	C4	−15.3	−16.7	5
Zea mays	C4	−20.9	−21.7	6
Zoysia japonica	C4	−24.1	−24.2	6
Miscanthus sinensis (1)	C4	−17.2	−17.3	6
Saccharum officinarum (1)	C4	−20.6	−20.7	6
Miscanthus sinensis (2)	C4	−17.5	−18.6	6
Saccharum officinarum (2)	C4	−20.0	−19.3	6
Sorghum bicolar	C4	−18.9	−19.6	6
Aristida adscensionis	C4	−24.9	−25.3	7
Aristida barbicollis	C4	−21.4	−23.9	7
Aristida congesta	C4	−22.9	−24.3	7
Aristida graciliflora	C4	−23.9	−24.1	7
Aristida meridionalis	C4	−22.4	−22.8	7
Aristida meridionalis	C4	−21.4	−21.9	7
Stipagrostis ciliata	C4	−21.7	−19.8	7
Stipagrostis hirtigluma	C4	−25	−23.2	7
Stipagrostis uniplumis	C4	−24.5	−25.9	7
Chloris gayana	C4	−22.5	−23.4	7
Chloris virgata	C4	−19.6	−20.2	7
Chloris virgata	C4	−20.6	−21.7	7
Enneapogon sp.	C4	−23	−22.7	7
Enneapogon cenchroides	C4	−19.4	−20.9	7
Enneapogon cenchroides	C4	−18.3	−20.1	7
Eragrostis nindensis	C4	−22.7	−24.6	7
Eragrostis superba	C4	−20.8	−21.8	7
Eragrostis tremula	C4	−25.1	−25.9	7
Eragrostis violacea de winter	C4	−18.1	−19.6	7
Eragrostis viscosa	C4	−19.6	−21.8	7
Schmidtia kalahariensis	C4	−22	−22.9	7
Sporobolus ioclados	C4	−21.8	−22.4	7
Sporobolus pyramidalis	C4	−22	−22.1	7
Bothriochloa insculpta	C4	−19.2	−18.7	7
Brachiaria erucitormis	C4	−20.4	−20.9	7
Digitaria milanjiana	C4	−18.9	−19.5	7
Hyparrhenia filipendula	C4	−21.9	−21.9	7
Loudetia simplex	C4	−18.6	−18.2	7
Panicum sp.	C4	−22.6	−23	7
Panicum arbusculum	C4	−22	−24	7
Panicum maximum	C4	−20.8	−19.4	7
Panicum maximum	C4	−24.2	−24.5	7
Themeda triandra	C4	−21.3	−19.6	7
Average		−21.4	−21.7	
SD		2.4	2.3	